JACS Au
AN OPEN ACCESS JOURNAL OF THE AMERICAN CHEMICAL SOCIETY

pubs.acs.org/jacsau

Article

Hydrogen Bond-Driven Order–Disorder Phase Transition in the Near-Room-Temperature Nonlinear Optical Switch $[Ag(NH_3)_2]_2SO_4$

Yi-Chang Yang, Xin Liu, Xue-Bin Deng, Li-Ming Wu,* and Ling Chen*

Cite This: *JACS Au* 2022, 2, 2059–2067

Read Online

ACCESS | Metrics & More | Article Recommendations | Supporting Information

ABSTRACT: Herein, we report a near-room-temperature nonlinear optical (NLO) switch material, $[Ag(NH_3)_2]_2SO_4$, exhibiting switching performance with strong room-temperature second harmonic generation (SHG) intensity that outperforms the UV–vis spectral region industry standard KH_2PO_4 (1.4 times stronger). $[Ag(NH_3)_2]_2SO_4$ undergoes a reversible phase transition (T_c = 356 K) from the noncentrosymmetric room-temperature phase ($P\bar{4}2_1c$, RTP) to a centrosymmetric high-temperature phase ($I4/mmm$, HTP) where both the SO_4^{2-} anions and $[Ag(NH_3)_2]^+$ cations are highly disordered. The weakening of hydrogen bond interactions in the HTP is also evidenced by the lower energy shift of the stretching vibration of the N–H···O bonds revealed by the *in situ* FT-IR spectra. Such weakening leads to an unusual negative thermal expansion along the *c* axis (−3%). In addition, both the atomic displacement parameters of the single-crystal diffraction data and the molecular dynamics-simulated mean squared displacements suggest the motions of the O and N atoms. Such a structural disorder not only hinders the phonon propagation and dramatically drops the thermal conductivity to 0.22 W m^{-1} K^{-1} at 361 K but also significantly weakens the optical anisotropy and SHG as verified by the DFT theoretical studies.

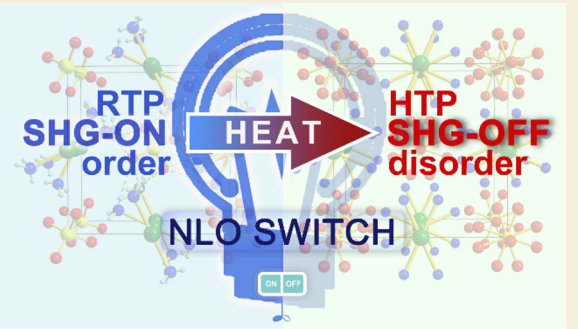

KEYWORDS: *nonlinear optical switch, disorder, hydrogen bond, phase transition, sulfate*

INTRODUCTION

Inorganic solid-state nonlinear optical (NLO) materials, as the key material of the all-solid-state laser devices, have been extensively studied and are widely applied in many fields, such as information processing, precision manufacturing, and telecommunications.[1−3] Among them, the second-order nonlinear optical materials showing the second harmonic generation (SHG) have greatly broadened the application range of nonlinear optics.[4] The NLO switch materials are potentially useful in applications such as sensors, information storage, and switching devices.[5,6] The switching between the SHG-on and SHG-off states under the external stimuli such as heat, light, pressure, etc., is associated with a reversible phase transition from a noncentrosymmetric (NCS, SHG-on state) to centrosymmetric (CS, SHG-off) structure.[7−9] However, such a phase transition is relatively rare, most of which is trigged by the structure conformation or orientation changes stimulated by the external stimuli,[8−11] and some are related to the disorder or rearrangement of atoms/groups in the structure.[8−13] The latter are found in some organic salts, such as $(Hdabco)(CF_3COO)$,[14] host–guest inclusion compounds, e.g., $(dipropylamine)(18\text{-crown-}6)ClO_4$,[15] and organic–inorganic hybrids, such as $(Me_3NNH_2)_2CdI_4$[16] and $(C_4H_{12}NO)MnCl_3$.[17] Previously, we report an inorganic NLO switch material, $K_x(NH_4)_{2-x}PO_3F$ (x = 0–0.3), showing the widest switching temperature range from 150 to 270 K benefiting from the continuously tunable T_c, which is adjustable by controlling the number of hydrogen bonds within the crystal structure.[18] Since the hydrogen bonding interaction is much weaker than ionic or covalent bonding interactions, the phase transition associated with the hydrogen bond interaction shall have a relatively small energy barrier. The most familiar phase transition is between the liquid H_2O and the ice. Another example is an industry standard material, KH_2PO_4 (KDP), which undergoes a phase transition driven by the hydrogen disordering above T_c = 123 K.[19,20] However, the inorganic groups are generally rigid and are less easily modified and less flexible than the organic species, and the inorganic NLO switch and its phase transition mechanism are relatively rare and challenging.

Herein, we discover a novel inorganic NLO switch material, $[Ag(NH_3)_2]_2SO_4$, that exhibits an excellent NLO switching performance near room temperature (T_c = 356 K). The *in situ* variable-temperature single-crystal X-ray diffraction data confirm that the order-to-disorder phase transition at 356 K

Received: June 16, 2022
Revised: July 20, 2022
Accepted: July 27, 2022
Published: August 12, 2022

https://doi.org/10.1021/jacsau.2c00353
JACS Au 2022, 2, 2059–2067

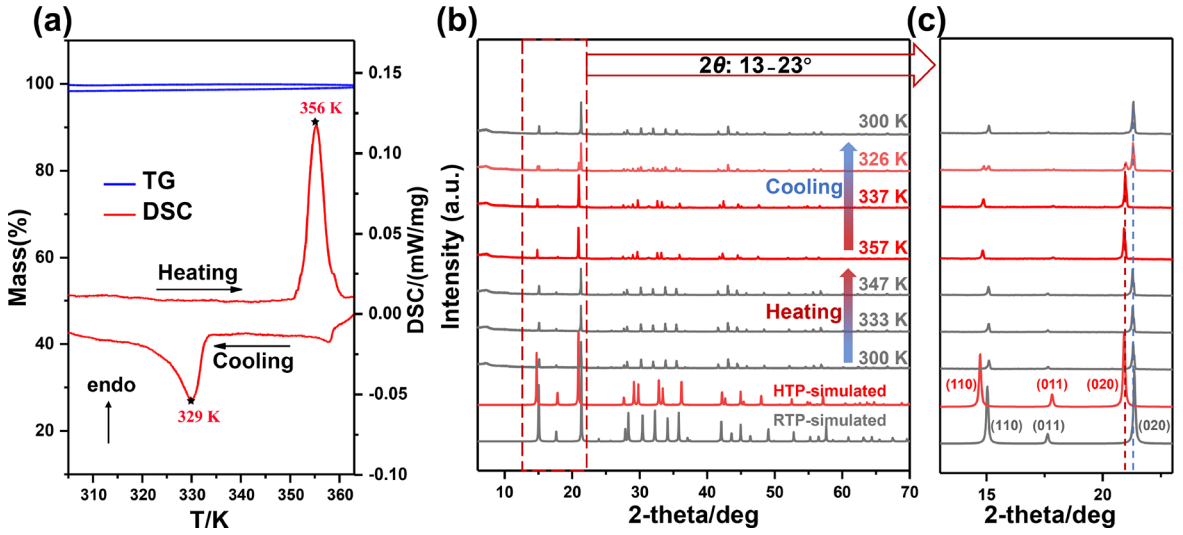

Figure 1. (a) DSC and TG curves of and (b) variable-temperature powder X-ray diffraction data of $[Ag(NH_3)_2]_2SO_4$. (c) Enlarged view of panel (b) in the 2θ range of 13−23°.

is reversible. Such a phase transition is associated with the weakening of the hydrogen bonds as evidenced by the stretching vibration energy change of the N−H···O bonds observed by the *in situ* FT-IR spectra. The disorders of the O and N atoms are revealed by both the atomic displacement parameters and the mean squared displacements by the molecular dynamics simulation. Such disorders hinder the phonon propagation and eventually decrease the thermal conductivity; meanwhile, such disorders weaken significantly the optical anisotropy and SHG according to the density functional theory (DFT) studies. These findings will further aid in the understanding of the mechanism of order−disorder phase transition and provide some insights into the future rational design of functional materials that are correlated with the phase transition, such as NLO switch, piezoelectric, and ferroelectric materials.

EXPERIMENTAL SECTION

Syntheses

The crystallographic structure of RTP $[Ag(NH_3)_2]_2SO_4$ was first determined in 1992 by Jacobs and Zachwieja,[21] and the room-temperature NLO property was first reported in 2021 by our group.[7] Herein, the syntheses followed the previous method, the 300 K single-crystal diffraction data agreed well with refs 7 and 21 (Tables S1−S3), and the *in situ* data collected at 313, 323, 333, 343, and 348 K were also determined to be RTP (Table S4) and those collected at 358 and 368 K were HTP (Tables S1−S5). All these new sets of single-crystal diffraction data are deposited in CCDC, with deposited numbers listed in Tables S1 and S4. In addition, by slow evaporation of saturated aqueous ammonia solution of Ag_2SO_4 at room temperature, large-sized single crystals of RTP $[Ag(NH_3)_2]_2SO_4$ with centimeter sizes (2.1 × 1.2 × 0.2 cm^3) were grown.

Structure Characterization

The single-crystal X-ray diffraction data were collected on a Bruker PHOTON II CPAD detector with a mirror-monochromatic INCOATEC IμS microfocus radiation source (50 kV per 1.4 mA). In addition, the temperature varied from room temperature to 366 K controlled by a CyroConnector with a liquid nitrogen mode. Data integration, cell refinement, and absorption corrections were carried out with the aid of SAINT. The crystal structures were solved by a direct method and refined through the full-matrix least-squares fitting on F^2 with the SHELX-2014 software package, the final refined solutions obtained were tested by the ADDSYM algorithm from PLATON, and no higher symmetries were found (Tables S1−S5). The powder X-ray diffraction data were collected using a Bruker Model D8 Advance powder diffractometer (Cu K_α radiation with λ = 1.5418 Å, 40 kV, and 40 mA) in the 2θ range of 10−70° with a scan step of 0.02°.

In Situ FT-IR Spectra

The *in situ* FT-IR spectra were measured on a Bruker Vertex 70v spectrophotometer in the region of 4000−800 cm^{-1} in an ammonia atmosphere. The sample was condensed with the annealed KBr into a pellet.

DSC Analyses

The differential scanning calorimetric (DSC) and thermal gravimetric (TG) data were collected by a NETZSCH STA 449 F5 thermal analyzer under a N_2 atmosphere. The sample was packed in Al_2O_3 crucibles and heated from 303 to 363 K at a rate of 1.0 K/min.

Thermal Diffusivity Analyses

Heat capacity (C_p) was measured by a TA Q2000 differential scanning calorimeter using sapphire as a reference material. The as-synthesized colorless polycrystalline sample was condensed by spark plasma sintering (SPS-211LX, Fuji Electronic Industrial Co., Ltd.) at 323 K for 30 min under a pressure of 50 MPa into a pellet of 1.03 mm in thickness and 10.00 mm in diameter. The density of the pellet was measured by Archimedes' method to be 2.608 g/cm^3 (94% of the theoretical density). Following the standard thermal diffusivity (λ) measurement procedure, a graphite coating was sprayed on the upper and bottom surfaces of the pellet, giving it a black appearance. The λ was measured on a NETZSCH LFA-457 instrument under a nitrogen atmosphere in the temperature range of 303−363 K.

Second Harmonic Generation

Variable-temperature SHG was measured using the standard Kurtz−Perry method. Polycrystalline samples with particle sizes of 150−212 μm were used to measure the SHG intensity at an incident 1064 nm wavelength under ambient conditions by a pump Nd:YAG laser with an energy of 2 mJ and a frequency of 2 Hz controlled by the RADIANT Tunable Laser System (OPOTEK, Inc.), and the measured temperature varied from 300 to 363 K controlled by an autothermostat (CXH902, Shanghai Changxin, Inc.).

Classical Molecular Dynamics (MD) Simulation and Theoretical Calculations

The classical MD simulations were performed using VASP with a Nose−Hoover thermostat[22−24] in a constant-volume and constant-temperature ensemble (NVT). For the RTP, the temperature was

https://doi.org/10.1021/jacsau.2c00353
JACS Au 2022, 2, 2059−2067

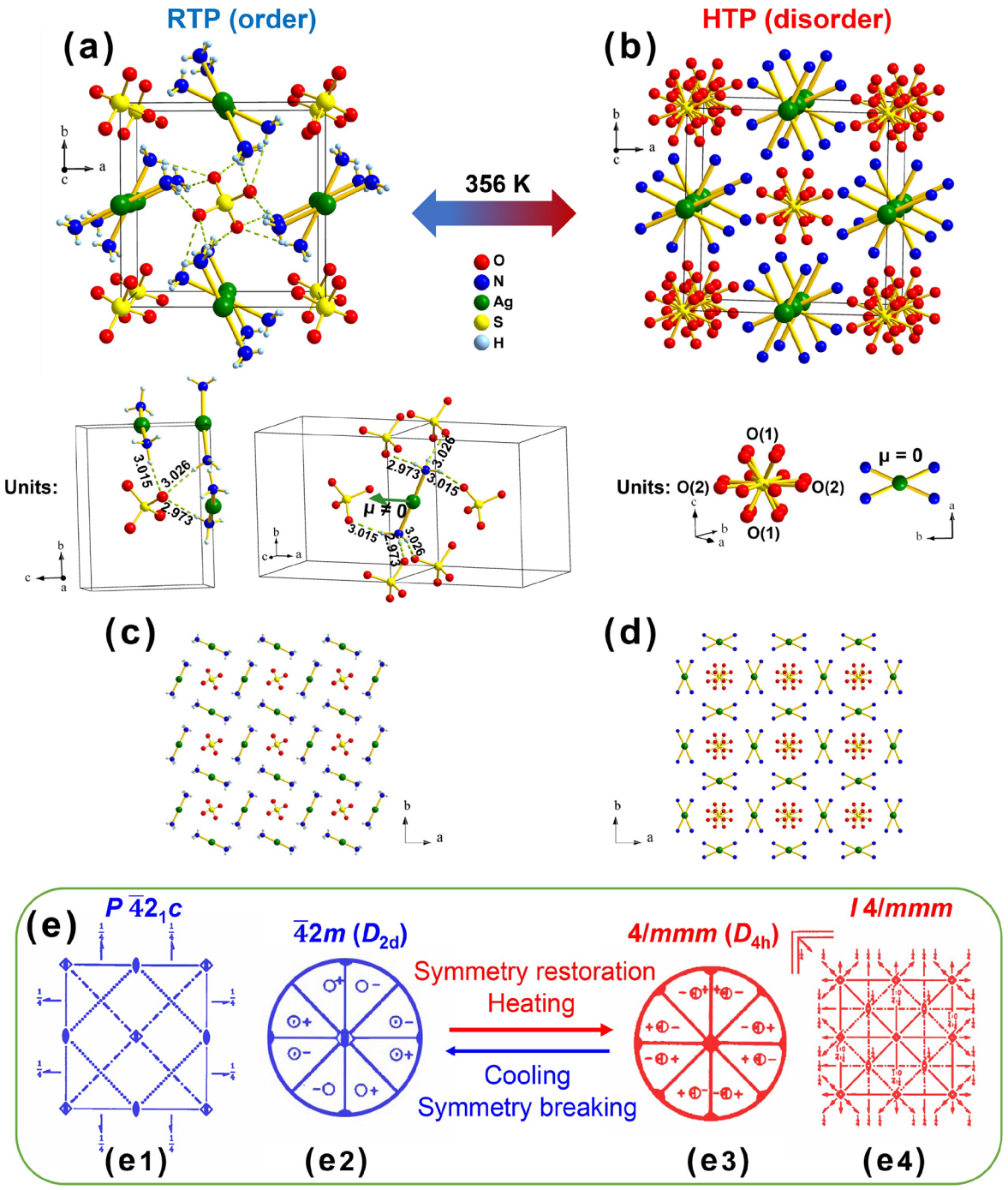

Figure 2. Crystal structures of (a) the RTP and (b) HTP (the hydrogen atoms are not drawn for clarity). Building units of the SO_4^{2-} anion and $[Ag(NH_3)_2]^+$ cation in the HTP (right) and RTP (left, with the major hydrogen bonds marked; μ: dipole moment). Single-layered structures of (c) the RTP and (d) HTP. (e) Spatial symmetry elements of (e1) the RTP and (e4) HTP and equatorial plane projections of (e2) $\bar{4}2m$ (D_{2d}) and (e3) $4/mmm$ (D_{4h}).

controlled at 298 K or 313−353 K with a 10 K step, 368 atoms were considered (i.e., within a 2 × 2 × 2 supercell), and a time step of 1 fs and 5000 total steps were utilized. Atomic mean square displacement and dynamic trajectory analysis were finished by the VMD program. To better understand the property difference between the HTP and the RTP, considering the complexity of disorder in the HTP, we regarded one of the frames in the MD equilibrium of an RTP 1 × 1 × 2 supercell as the approximate structure of HTP, in which the orientation of each SO_4^{2-} anion is as opposite as possible and that of $[Ag(NH_3)_2]^+$ is as random as possible to mimic the real situation in the HTP (Figure S1). Subsequently, with such an approximation containing 92 atoms in total, the relevant properties of $HTP^{approx.}$ are calculated based on DFT by using the pseudopotential method in the VASP package.[25,26] Generalized gradient approximation (GGA)[27] was chosen as the exchange correlation functional, and a plane-wave basis with projector augmented wave (PAW)[28] potentials was used. A kinetic energy cutoff of 500 eV was chosen with Monkhorst−Pack k-point meshes spanning less than 0.05/Å^3 in the Brillouin zone. The static self-consistency, the density of state, and the energy band with a dense 0.02/Å^3 k-point spacing mesh were calculated. According to the Kramers−Kronig transformation,[29,30] the real part of the dielectric function $\varepsilon_1(\omega)$, refractive indices (n), and birefringence (Δn) were calculated based on the so-called length-gauge formalism derived by

https://doi.org/10.1021/jacsau.2c00353
JACS Au 2022, 2, 2059−2067

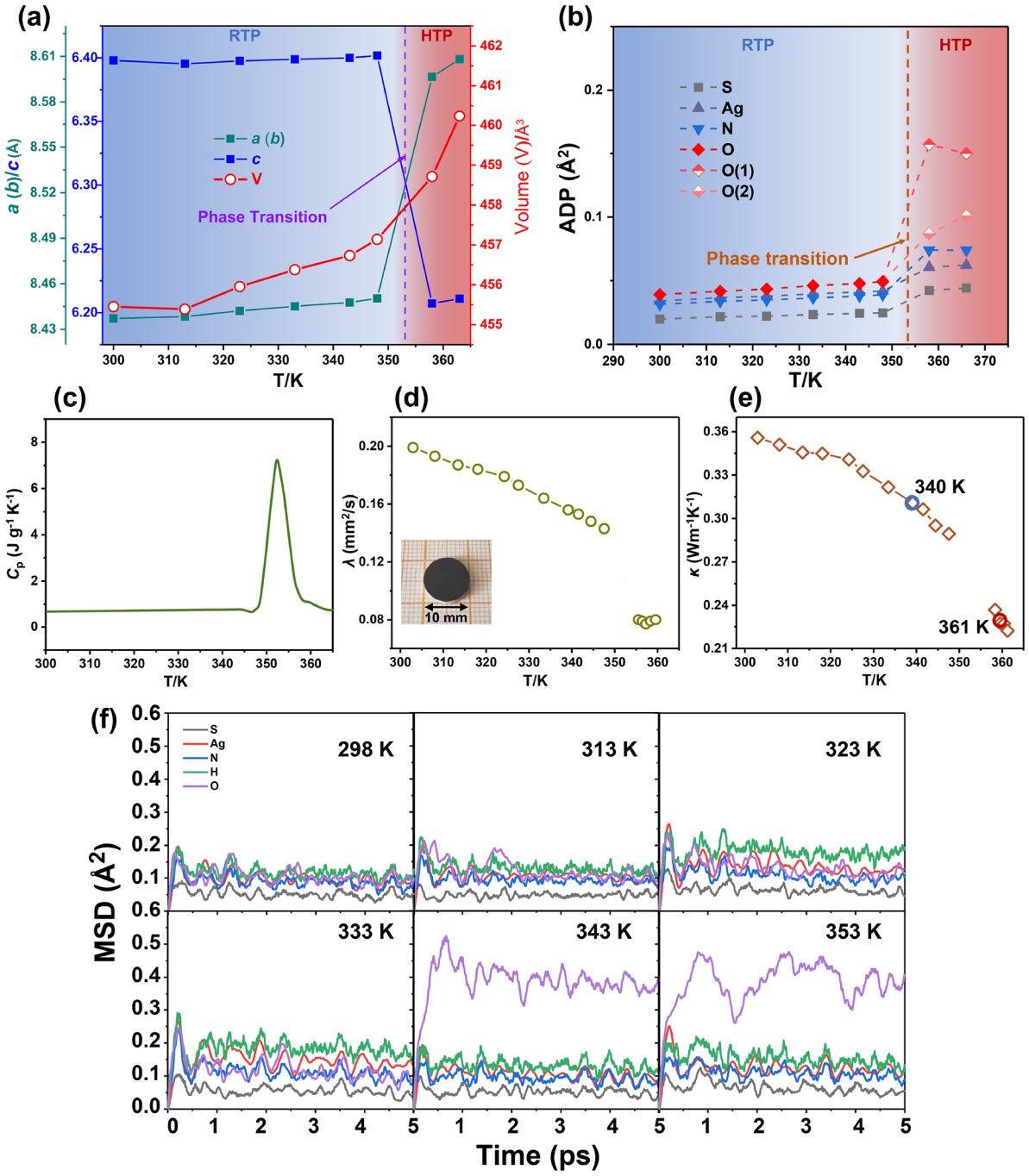

Figure 3. (a) Unit cell parameters of $[Ag(NH_3)_2]_2SO_4$ vary with temperature. (b) Atomic displacement parameters (ADPs) in the temperature range of 300−366 K. (c) Heat capacity (C_p) measured by DSC and (d) thermal diffusivity (λ) measured by the laser flash method. Inset: photo of the condensed polycrystalline sample with a graphite coating on the upper and bottom surfaces. (e) Temperature dependence of thermal conductivity (κ) calculated by $\kappa = C_p \times d \times \lambda$, where d is the density. The data near the RTP-to-HTP phase transition in panels (d) and (e) are not considered. (f) MSDs of individual atoms over the total time span calculated for six different temperatures from 298 to 353 K.

Aversa and Sipe,[31,32] utilizing the specific calculation method of Zhang et al.;[33] the SHG coefficients were also calculated.

RESULTS AND DISCUSSION

Thermal Analyses and Variable-Temperature Powder X-ray Diffractions

The simultaneous differential scanning calorimetry (DSC) thermal analyses were performed to characterize the phase transition of compound $[Ag(NH_3)_2]_2SO_4$ (Figure 1a). As shown, a first-order phase transition at 356 K without any weight loss is observed in the heating run, which is accompanied by an exothermic peak at 329 K in the cooling run with a large thermal hysteresis of 27 K. The corresponding entropy change ΔS is estimated by the Clausius equation[18] $\Delta S = \int_{T_1}^{T_2} \frac{Q}{T} dT \approx \frac{\Delta H^{exp}}{T_c}$; the ΔS is calculated to be 22.48 J mol^{-1} K^{-1} during the heating run. According to the Boltzmann equation $\Delta S = R \ln N$, where R is the gas constant and N is the multiplicity of microscopic states, the N is calculated to be 14.94, which is remarkably larger than that of some of the

https://doi.org/10.1021/jacsau.2c00353
JACS Au 2022, 2, 2059−2067

inorganic or inorganic−organic hybrid NLO switch material systems, for instance, 1.30 in $K_x(NH_4)_{2-x}PO_3F$,[18] 4.15 in bis(2-chloroethyl)amine hydrochloride,[34] 2.31 in $[NH_3(CH_2)_5NH_3]SbCl_5$,[12] and 1.94 in $[H_2dabcoCl_2]$-$[FeCl_3(H_2O)_3]$.[35] Yet, the N of the title compound is smaller than 20.23 in the organic complex 2-(hydroxymethyl)-2-nitro-1,3-propanediol.[36] The large entropy change and large N value suggest that upon heating, the RTP of $[Ag(NH_3)_2]_2SO_4$ transforms into a state of large entropy where the atoms adopt a large number of different states that are accessible with the exact same probability. In short, regarding the structural disorder, the HTP shall be highly disordered.

To further verify the phase transition, variable-temperature powder X-ray diffraction data were collected on the tetrahedral $[Ag(NH_3)_2]_2SO_4$ polycrystalline powders. As shown in Figure 1b,c, the PXRD patterns are the same at 300, 333, and 347 K, as indicated by the identical position of the (110) and (020) peaks, which start to shift at 357 K to a lower 2θ angle simultaneously, and the (011) reflection peak shifts to a higher 2θ angle. The lower angle shift of the (110) and (020) reflections indicates an increase in (110)- and (020)-interplanar distances, whereas the higher angle shift of the (011) reflections indicates a decrease in (011)-interplanar distance. Considering the tetrahedral symmetry of RTP $[Ag(NH_3)_2]_2SO_4$, such shifts suggest an expansion in the a and b axes and a decrease in the c axis. When the temperature goes above 357 K, some new reflection peaks are seen at 2θ = 28.5, 29.2, 32.2, and 32.8. When the temperature drops to 326 K, the (110) and (020) peaks are seen to shift and eventually shift back at 300 K to the original positions at 15° and 22°, respectively (Figure 1c). Note that the coexistence of two (110) and two (020) peaks is observed in the pattern collected at 326 K, which may indicate the coexistence of two phases. In the end, the temperature drops to 300 K and the peaks of the HTP disappear. Thus, a phase transition of $[Ag(NH_3)_2]_2SO_4$ is verified by the VT powder X-ray diffraction data, which are well consistent with the DSC results (Figure 1).

Crystal Structure Comparisons and Hydrogen Bond Weakening-Driven Phase Transition

The RTP single-crystal diffraction data of $[Ag(NH_3)_2]_2SO_4$ were recollected at 300 K, which agree well with the previous reports.[7,21] The diffraction data were also collected at 313−348 K with a 10° step, which are well solved as the tetragonal $P\bar{4}2_1c$ RTP phase (Figure 2a and Table S4). Yet, at higher temperatures of 358 and 366 K, we observed a different tetragonal structure featuring centrosymmetric $I4/mmm$ with cell parameters of $a = b = 8.6081(11)$ Å and $c = 6.2110(8)$ Å (Table S1). Compared with the unit cell of the RTP, a negative expansion of the c axis (−3%) but positive expansions of the a/b axis (+1.73%) are observed, which lead to a normal positive unit cell expansion (+0.34%) from the RTP to HTP (Figure 3a). The negative c axis expansion agrees with the (011) reflection shifting toward a higher 2θ angle as the temperature increases, and the positive a/b axis expansions are consistent with the lower 2θ angle shift of the (110) and (020) peaks (Figure 1). As listed in Tables S2 and S5, in the RTP structure, the SO_4^{2-} anions and $[Ag(NH_3)_2]^+$ cations are ordered with full occupancy. Characteristically, each O atom of a SO_4 tetrahedron is connected to the cation via three strong N−H···O hydrogen bonds with a N···O distance of 2.97−3.03 Å (Figure 2a). On the other hand, each N end of the $[Ag(NH_3)_2]^+$ cation is fixed onto a matrix of the SO_4^{2-} anion through such hydrogen bonds via a motif in which the linear stick-like cation bends with a N−Ag−N angle = 174° pointing to the opposite direction of the slightly weaker N−H···O hydrogen bond with a N···O distance of 3.03 Å (Figure 2a). Consequently, each individual $[Ag(NH_3)_2]^+$ cation carries a small dipole moment that contributes greatly to the anisotropy[7] of the material. The structure packing along the c direction and a single-layered structure of the RTP are shown in Figure S3 and Figure 2c, respectively.

Differently, in the structure of the HTP, the SO_4^{2-} anions and $[Ag(NH_3)_2]^+$ cations become severely disordered (Figure 2b). The structure packing along the c direction and a single-layered structure of the HTP are shown in Figure S3 and Figure 2d, respectively. As listed in Table S5, the O atom at the Wyckoff 8e site in the RTP structure moves upon the heat stimulation above 358 K to either a 16m site (O1, occ. of 25%) or a 16l site (O2, occ. of 25%). Meanwhile, the N atom also leaves the 8e Wyckoff site in the RTP and disorders over the 16l Wyckoff site with an occ. of 50% (Table S2). Such disorders indicate that O and N atoms in the HTP have large distribution possibilities, giving the structure a large entropy that is coincident with the thermal analyses and the results estimated by the Clausius equation and Boltzmann equation discussed above. As shown in Figure 2b, such disorders give a multiple orientational possibility of the SO_4 tetrahedron, which consequently presents an average configuration in the HTP rather than a typical tetrahedral configuration in the RTP. In comparison, the disorder of the linear stick-like $[Ag(NH_3)_2]^+$ cation is nearly confined within the (001) plane, and the N−Ag−N angle is 180° in the HTP (Figure 2b, Figure S3d, and Tables S3 and S5). Nevertheless, the temperature dependences of the atomic displacement parameter of both the RTP and HTP show a normal increase in the thermal vibration of each atom upon the increase in temperature (Figure 3b).

To further understand the occurrence of the center of symmetry during such an order (RTP, NCS)-to-disorder (HTP, CS) phase transition, the symmetry elements are illustrated (Figure 2e). The $\bar{4}$ axis in the RTP located at the middle of the unit cell pointing to the paper rotates a $[Ag(NH_3)_2]^+$ cation 90° on the ab plane and subsequently inverts it to the position where the dipole moment is thus oppositely directed (Figure S2a), whereas in the HTP, the N−Ag−N angle of the cation is 180°, and four such cations are operated by a 4 axis (Figure S2b), where an inversion center appears. As detailed in Figure 2e, the HTP involves 16 symmetry elements (E, $2C_4$, C_2, $2C_2'$, $2C_2''$, i, $2S_4$, σ_h, $2\sigma_v$, and $2\sigma_d$) with the point group $4/mmm$ (D_{4h}), whereas the RTP involves much less symmetry elements, which are only eight (E, C_2, $2C_2'$, $2S_4$, and $2\sigma_d$) with the point group $\bar{4}2m$ (D_{2d}). Such a symmetry element decrease consists in the Landau phase transition theory prediction when a structure transforms from high symmetry down to low symmetry. The RTP-to-HTP transition is driven by the structural disorder of both the SO_4^{2-} tetrahedral anions and the linear stick-like $[Ag(NH_3)_2]^+$ cations. As shown in Figure 2a, because of the constraint of the strong NH···O hydrogen bonds that glue the individual stick-like $[Ag(NH_3)_2]^+$ cations onto the matrix formed by individual SO_4^{2-} anions, the number of symmetry elements in the RTP is therefore less than that in the HTP. Such a transition is different from the majority of the hybrid NLO switch compounds, for instance, $(Hdabco)ClO_4$,[37] in which only the flexible organic species is the rotational moiety. In $[Ag(NH_3)_2]_2SO_4$, however, both the cation and anion are

https://doi.org/10.1021/jacsau.2c00353
JACS Au 2022, 2, 2059−2067

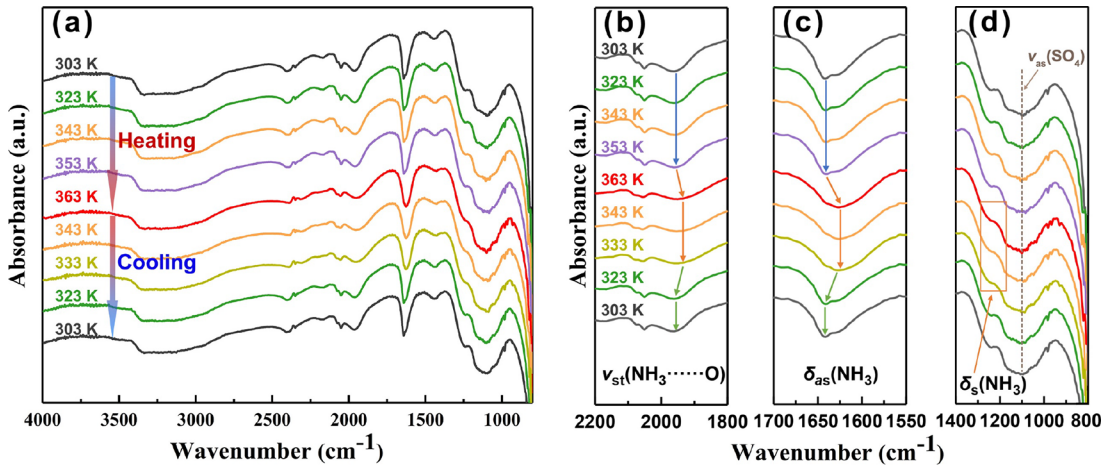

Figure 4. (a) *In situ* FT-IR spectra of $[Ag(NH_3)_2]_2SO_4$ from 303 to 363 K. Partially enlarged views of (b) $\nu_{st}(NH_3\cdots O)$ (~1940−1961 cm^{-1}), (c) $\delta_{as}(NH_3)$ (~1625−1641 cm^{-1}), and (d) $\delta_s(NH_3)$ (~1243 cm^{-1}); inset orange box: flattening of the $\delta_s(NH_3)$ peak of the HTP; dashed line: $\nu_{as}(SO_4)$ (~1107 cm^{-1}).

rotational, which gives a large multiplicity of microscopic states and leads to a large entropy during the phase transition (Figure 1).

As shown in Figure 3a, during the RTP-to-HTP phase transition, $[Ag(NH_3)_2]_2SO_4$ exhibits an unusually negative expansion in the *c* direction (−3%), the origin of which is very alluring. The detailed structure analyses suggest that the projected $Ag-N^{projected}$ lengths on the *a* (or *b*) axis in the RTP and HTP are 1.895 and 1.866 Å, respectively (Figure S4 and Table S6). More significantly, during the phase transition, the N−Ag−N angle changes from 174° to 180°. As we know, in the $[Ag(NH_3)_2]^+$ cation, the Ag^+ ion provides an empty sp-hybrid orbital, and the NH_3 molecule donates an electron pair so as to form a directional covalent bond. As for the flattening of the N−Ag−N angle, the Ag^+-sp-hybrid orbital has a better overlap with the N-$2s^2$-electron pair, which is verified by the Ag−N bond shortening (2.107 Å vs 2.066 Å) that infers a decrease in the effective positive charge of the Ag^+ ion.[38,39] Consequently, the repulsion between Ag-cations is weakened as implied by the Ag−Ag distance shortening (3.1990 Å vs 3.1055 Å). Such a hydrogen bonding weakening-driven negative thermal expansion (along the *c* axis, −3%) is unique and rare.[40]

In addition, the atomic displacement parameters (ADPs) also demonstrate the order−disorder phase transition (Figure 3b). The ADPs of all atoms increase slowly with the temperature before and increase obviously after the phase transition due to the splitting of the O atom from one 8*e* Wyckoff site into two Wyckoff sites of 16*m* (O1) and 16*l* (O2).

Further, the thermal conductivity of $[Ag(NH_3)_2]_2SO_4$ was measured in the temperature range of 303 to 363 K (Figure 3c−e). The total thermal conductivity (κ) constitutes the lattice thermal conductivity (κ_{lat}) and electric thermal conductivity (κ_{ele}), and the κ_{ele} is almost zero owing to its insulator nature with a large band gap (E_g = 4.42 eV[7]), so the thermal conductivity of $[Ag(NH_3)_2]_2SO_4$ is mainly determined by κ_{lat}. As heat transport in a crystalline solid is governed by the propagation and scatterings of phonons through the lattice,[41] the measured temperature dependence of the thermal diffusivity (λ) shows a slow decrease before the phase transition, which is related to the phonon scattering increasing as the temperature increases. After the phase transition, the λ significantly decreases. The κ is calculated to be 0.31 W m^{-1} K^{-1} at 340 K and decreases to 0.22 W m^{-1} K^{-1} at 361 K (Figure 3e). Such a κ decrease reveals additional thermal resistance that may come from the phonon confinement and phonon focusing[42,43] due to the structural disordering structure in the HTP, and such a disorder-induced low λ is also seen in some liquid-like thermoelectric materials, such as argyrodite Ag_9GaSe_6.[44]

In Situ FT-IR Spectra

Limited by the best facility we have currently, it is still difficult to produce extremely high-quality single crystals of HTP $[Ag(NH_3)_2]_2SO_4$, and the refinement of the single-crystal diffraction data cannot directly solve the positions of hydrogen atoms in the HTP structure (Tables S1−S5). Indeed, considering the severe disorder in such a structure, any attempt would be in vain. To further understand the role of the hydrogen bond during the phase transition, the *in situ* FT-IR spectra were measured in the temperature range of 303 to 363 K and then from 363 to 303 K (Figure 4a). As the temperature rises from 303 to 353 K, the vibrations of $\nu_{st}(NH_3\cdots O)$ and $\delta_{as}(NH_3)$ remain at 1961 and 1641 cm^{-1}, respectively, but move to lower energies of 1940 and 1625 cm^{-1} at 363 K, which are in accordance with the phase transition occurrence from 353 to 363 K (Figure 4b,c). Importantly, these lower vibration energy shifts of $(NH_3\cdots O)$ and N−H confirm the weakening of hydrogen bonds during the RTP-to-HTP transition. When the temperature finally drops below 333 K, the vibrations of $\nu_{st}(NH_3\cdots O)$ and $\delta_{as}(NH_3)$ return to the original positions, which indicates a reversible phase transition. In addition, the $\delta_s(NH_3)$ at 1243 cm^{-1} is obviously visible in the RTP but almost flattened in the HTP, which also reflects the violent motion of the group within the lattice[34] (Figure 4d), and the peaks of $\nu_{as}(SO_4)$ (~1107 cm^{-1}) do not move noticeably, which may indicate that the SO_4^{2-} anion is only spatially disordered and the S−O bond length has not obviously changed.

SHG Switching Performance

Above T_c, the weakening of the hydrogen bond in $[Ag(NH_3)_2]_2SO_4$ drives an ordered-to-disordered structure transition, leading to switching from the SHG-on state to the SHG-off state. The SHG intensity was measured by a standard Kurtz−Perry method on polycrystalline samples with particle

https://doi.org/10.1021/jacsau.2c00353
JACS Au 2022, 2, 2059−2067

sizes of 150−212 μm.[7] As shown in Figure 5a, the RTP (SHG-on state) exhibits a strong SHG signal (1.4 × KDP), whereas

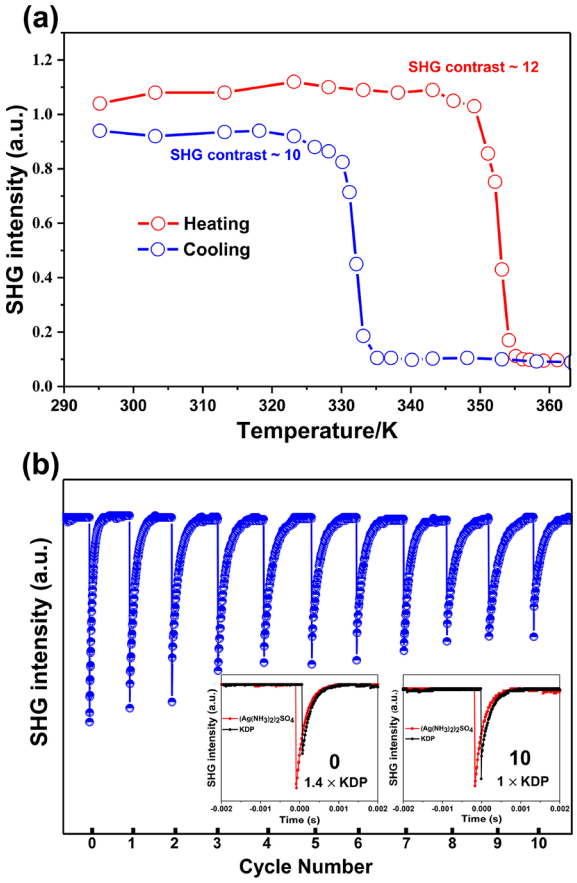

Figure 5. (a) Temperature-dependent SHG intensity of $[Ag(NH_3)_2]_2SO_4$ during heating and cooling. (b) SHG intensity comparison between the repetitive transition of the RTP (SHG-on) and HTP (SHG-off) during 10 cycles. Inset: SHG signals of cycle numbers 0 and 10.

above T_c, the HTP (SHG-off state) exhibits an almost zero SHG signal (that is nothing but the weak noise error of the instrument). Such experimental data give an SHG contrast of 12 that is defined as contrast = $(\text{SHG intensity})_{\text{on-state}}/(\text{SHG intensity})_{\text{off-state}}$. (Caution: The absolute value of the contrast does not represent the intrinsic nature of the switch material. For instance, for the cases where the off-state is a centrosymmetric structure as we reported herein, the $(\text{SHG intensity})_{\text{off-state}}$ is zero; theoretically, the contrast shall be infinite!) In the following cooling process, the SHG signal switches on when the temperature is below 328 K and gives a contrast of ∼10, indicating that the SHG response is reversible with a temperature hysteresis that is consistent with the DSC results. The SHG intensity of $[Ag(NH_3)_2]_2SO_4$, 1.4 times stronger than that of KDP, is one of the strongest among the known solid-state SHG switches, such as $[CH_3(CH_2)_3NH_3]_2(CH_3NH_3)Pb_2Br_7$ (0.4 × KDP),[45] $[C_4H_{10}N][CdCl_3]$ (0.4 × KDP),[10] [isoQH]ReO_4 (0.5 × KDP),[46] $(Hdabco^+)(CF_3COO^-)$ (0.8−1.2 × KDP),[14] and $K_{0.3}(NH_4)_{1.7}PO_3F$ (1.1 × KDP).[18] In addition to the strong SHG intensity and the large on−off contrast, $[Ag(NH_3)_2]_2SO_4$ exhibits very good reversible capacity; after switching on and off for 10 cycles, the SHG intensity in principle is retained well (Figure 5b), which is superior to the photochromic SHG switchable polymers[47,48] or Langmuir−Blodgett thin films,[49] which usually repeat less than five cycles.

Classical Molecular Dynamics Simulation and DFT Optical Property Calculations

To further understand the micro-origin at the atomic level of the $[Ag(NH_3)_2]_2SO_4$ phase transition, the MD simulation was carried out. As an important parameter to study the phase transition,[50] the mean squared displacement (MSD) is analyzed (Figure 3f). The MSD of an individual atom shows a slow rising and chaotic trend from 298 to 333 K, and then that of the O atom dramatically increases after 343 K and remains at the high level at 353 K, which indicates a T_c in the range of 333 to 343 K that is about 10−20 K lower than the experimental value (356 K). The MD trajectories of all atoms at 353 K are considerably broader than those at 298 K, indicating a serious disorder in HTP, which to some extent supports the refinement results of single-crystal diffraction data (Figure S5).

Complicated by the severe disorder in the HTP, the full theroretical calculation is impossible; thus, only an approximate (denoted as $HTP^{approx.}$) is utilized in the corresponding electronic structures and the linear and nonlinear optical property calculations (Figure S6). The calculated band gap of $HTP^{approx.}$ is 2.65 eV, lower than 2.93 eV of RTP (Figure S6a,b). More importantly, the calculated refractive indices are RTP ($n_x = n_y = 1.541$ and $n_z = 1.643$) and $HTP^{approx.}$ ($n_x = 1.553$, $n_y = 1.557$, and $n_z = 1.629$) (Figure S6c), giving an increase in the x and y directions but a decrease in the z direction, and eventually lead to a birefringence (Δn) decrease from the RTP (0.102) to $HTP^{approx.}$ (0.076) (Figure S6d). These results support well the crystallographic structure difference. The calculated polarizability anisotropy ($\Delta\alpha$) of the $[Ag(NH_3)_2]^+$ cation is 12.84, overwhelming that of the SO_4^{2-} anion ($\Delta\alpha$ = 0.0093),[7] which indicates that the anisotropy of $[Ag(NH_3)_2]_2SO_4$ mainly originates from the c direction-bending linear stick-like $[Ag(NH_3)_2]^+$ cation. As shown in Figure S7, in the $HTP^{approx.}$, the disorder makes the dipoles randomly oriented, and the flattening of the N−Ag−N angle diminishes the numerical magnitude of the dipole moment, which results in a decrease in anisotropy and eventually a Δn decrease from the RTP to $HTP^{approx.}$ The anisotropy decrease in the $HTP^{approx.}$ is consistent with its highly disordered structure feature. Please keep in mind that the $HTP^{approx.}$ differs from the real disordered structure, and the $HTP^{approx.}$ remains a long-range ordered structure feature to facilitate the corresponding calculations; there must be a certain deviation from the real refractive index. The same is true for the calculated d_{36}, which is 0.45 pm/V at 1064 nm of the $HTP^{approx.}$, significantly smaller than that of the RTP (1.50 pm/V) (Figure S6e). With the aid of these calculations, it is reasonable to conclude that the SHG coefficient of the centrosymmetric HTP is zero and the birefringence will be smaller than that of the approximation (0.076).

CONCLUSIONS

In summary, a novel near-room-temperature inorganic NLO switch material, $[Ag(NH_3)_2]_2SO_4$, is discovered, which shows a phase transition (T_c) at 356 K and exhibits excellent NLO switch performance, including a strong SHG response (1.4 × KDP), remarkable SHG contrast (∼10), and good reversibility (>10 cycles). The NCS room-temperature phase (RTP) that transforms into a CS HTP is first reported, which is driven by

https://doi.org/10.1021/jacsau.2c00353
JACS Au 2022, 2, 2059−2067

the severe disorder of the SO_4^{2-} anions and $[Ag(NH_3)_2]^+$ cations. The hydrogen bond interaction between anions and cations is greatly weakened as confirmed by the lower energy shift of the vibrations of $(NH_3\cdots O)$ and N−H bonds above T_c. In addition, the profound motion of the O atoms and the less profound motion of N atoms during the phase transition are demonstrated by the ADPs and MSDs. Furthermore, the structure disorder hinders the phonon propagation and eventually decreases the thermal conductivity and weakens the birefringence and SHG coefficients of the HTP compared to the RTP. These studies verify that the structural disorder significantly weakens the optical anisotropy and SHG response. We believe that these discoveries will further aid in the understanding of the mechanism of order−disorder phase transition and provide useful insights into the future design and synthesis of functional materials that are correlated with the phase transition.

■ ASSOCIATED CONTENT

Supporting Information

The Supporting Information is available free of charge at https://pubs.acs.org/doi/10.1021/jacsau.2c00353.

Details of crystallography data, additional crystal structure figures, and calculation results including band structures, refractive index, birefringence, and frequency-dependent SHG coefficients (PDF)

List of all CIF files of the single crystals (ZIP)

■ AUTHOR INFORMATION

Corresponding Authors

Li-Ming Wu − *Beijing Key Laboratory of Energy Conversion and Storage Materials, College of Chemistry, Beijing Normal University, Beijing 100875, People's Republic of China; Center for Advanced Materials Research, Beijing Normal University, Zhuhai 519087, People's Republic of China;* orcid.org/0000-0001-8390-2138; Email: wlm@bnu.edu.cn

Ling Chen − *Beijing Key Laboratory of Energy Conversion and Storage Materials, College of Chemistry, Beijing Normal University, Beijing 100875, People's Republic of China; Center for Advanced Materials Research, Beijing Normal University, Zhuhai 519087, People's Republic of China;* orcid.org/0000-0002-3693-4193; Email: chenl@bnu.edu.cn

Authors

Yi-Chang Yang − *Beijing Key Laboratory of Energy Conversion and Storage Materials, College of Chemistry, Beijing Normal University, Beijing 100875, People's Republic of China*

Xin Liu − *Beijing Key Laboratory of Energy Conversion and Storage Materials, College of Chemistry, Beijing Normal University, Beijing 100875, People's Republic of China;* orcid.org/0000-0003-3622-0446

Xue-Bin Deng − *Beijing Key Laboratory of Energy Conversion and Storage Materials, College of Chemistry, Beijing Normal University, Beijing 100875, People's Republic of China*

Complete contact information is available at: https://pubs.acs.org/10.1021/jacsau.2c00353

Author Contributions

The manuscript was written through contributions of all authors. CRediT: **Yi-Chang Yang** data curation, formal analysis, investigation, resources, writing-original draft; **Xin Liu** writing-original draft; **Xue-Bin Deng** formal analysis, software; **Li-Ming Wu** conceptualization, formal analysis, funding acquisition, investigation, methodology, project administration, resources, software, supervision, validation, visualization, writing-original draft, writing-review & editing; **Ling Chen** conceptualization, data curation, formal analysis, funding acquisition, investigation, project administration, resources, supervision, validation, writing-original draft, writing-review & editing.

Notes

The authors declare no competing financial interest.

■ ACKNOWLEDGMENTS

This research was supported by the National Natural Science Foundation of China (22193043 and 21971019).

■ REFERENCES

(1) Dini, D.; Calvete, M. J. F.; Hanack, M. Nonlinear Optical Materials for the Smart Filtering of Optical Radiation. *Chem. Rev.* **2016**, *116*, 13043−13233.

(2) Xu, J.; Li, X.; Xiong, J.; Yuan, C.; Semin, S.; Rasing, T.; Bu, X. Halide Perovskites for Nonlinear Optics. *Adv. Mater.* **2020**, *32*, 1806736.

(3) Maczka, M.; Zareba, J. K.; Gagor, A.; Stefanska, D.; Ptak, M.; Roleder, K.; Kajewski, D.; Soszynski, A.; Fedoruk, K.; Sieradzki, A. $[Methylhydrazinium]_2PbBr_4$, a Ferroelectric Hybrid Organic-Inorganic Perovskite with Multiple Nonlinear Optical Outputs. *Chem. Mater.* **2021**, *33*, 2331−2342.

(4) Chen, J.; Hu, C.-L.; Kong, F.; Mao, J.-G. High-Performance Second-Harmonic-Generation (SHG) Materials: New Developments and New Strategies. *Acc. Chem. Res.* **2021**, *54*, 2775−2783.

(5) Ye, H.-Y.; Tang, Y.-Y.; Li, P.-F.; Liao, W.-Q.; Gao, J.-X.; Hua, X.-N.; Cai, H.; Shi, P.-P.; You, Y.-M.; Xiong, R.-G. Metal-Free Three-Dimensional Perovskite Ferroelectrics. *Science* **2018**, *361*, 151−155.

(6) Castet, F.; Rodriguez, V.; Pozzo, J.-L.; Ducasse, L.; Plaquet, A.; Champagne, B. Design and Characterization of Molecular Nonlinear Optical Switches. *Acc. Chem. Res.* **2013**, *46*, 2656−2665.

(7) Yang, Y.-C.; Liu, X.; Lu, J.; Wu, L.-M.; Chen, L. $[Ag(NH_3)_2]_2SO_4$: A Strategy for the Coordination of Cationic Moieties to Design Nonlinear Optical Materials. *Angew. Chem., Int. Ed.* **2021**, *60*, 21216−21220.

(8) Zhang, S.-Y.; Shu, X.; Zeng, Y.; Liu, Q.-Y.; Du, Z.-Y.; He, C.-T.; Zhang, W.-X.; Chen, X.-M. Molecule Based Nonlinear Optical Switch with Highly Tunable On-off Temperature using a Dual Solid Solution Approach. *Nat. Commun.* **2020**, *11*, 2752.

(9) Jiang, D.; Jiang, Z.; Song, H.; Wang, P.; Luo, H.; Li, C.; Liu, K.; Wen, T.; Yang, W.; Zhao, Y.; Wang, Y. Pressure Controls the Structure and Nonlinear Optical Properties of Piezochromic $CdTeMoO_6$. *Chem. Mater.* **2021**, *33*, 2929−2936.

(10) Xu, W.-J.; He, C.-T.; Ji, C.-M.; Chen, S.-L.; Huang, R.-K.; Lin, R.-B.; Xue, W.; Luo, J.-H.; Zhang, W.-X.; Chen, X.-M. Molecular Dynamics of Flexible Polar Cations in a Variable Confined Space: Toward Exceptional Two-Step Nonlinear Optical Switches. *Adv. Mater.* **2016**, *28*, 5886−5890.

(11) Li, L.; Sun, Z.; Ji, C.; Zhao, S.; Luo, J. Rational Design and Syntheses of Molecular Phase Transition Crystal Materials. *Cryst. Growth Des.* **2016**, *16*, 6685−6695.

(12) Mei, G.-Q.; Zhang, H.-Y.; Liao, W.-Q. A Symmetry Breaking Phase Transition-Triggered High-Temperature Solid-State Quadratic Nonlinear Optical Switch Coupled with a Switchable Dielectric Constant in an Organic-Inorganic Hybrid Compound. *Chem. Commun.* **2016**, *52*, 11135−11138.

(13) Wang, Y.; Zhang, T.; Lun, M.-M.; Zhou, F.-L.; Fu, D.-W.; Zhang, Y. Halogen Regulation Triggers NLO and Dielectric Dual Switches in Hybrid Compounds with Green Fluorescence. *Inorg. Chem. Front.* **2021**, *8*, 4230−4238.
(14) Sun, Z.; Luo, J.; Zhang, S.; Ji, C.; Zhou, L.; Li, S.; Deng, F.; Hong, M. Solid-State Reversible Quadratic Nonlinear Optical Molecular Switch with an Exceptionally Large Contrast. *Adv. Mater.* **2013**, *25*, 4159−4163.
(15) Ji, C.; Sun, Z.; Zhang, S.; Zhao, S.; Chen, T.; Tang, Y.; Luo, J. A Host-Guest Inclusion Compound for Reversible Switching of Quadratic Nonlinear Optical Properties. *Chem. Commun.* **2015**, *51*, 2298−2300.
(16) Zeng, Y.; Hu, C.-L.; Xu, W.-J.; Zeng, T.-W.; Zhu, Z.-X.; Chen, X.-X.; Liu, D.-X.; Chen, Y.-J.; Zhang, Y.-B.; Zhang, W.-X.; Chen, X.-M. An Exceptional Thermally Induced Four State Nonlinear Optical Switch Arising from Stepwise Molecular Dynamic Changes in a New Hybrid Salt. *Angew. Chem., Int. Ed.* **2022**, *134*, e202110082.
(17) Hua, X.-N.; Zhang, W.-Y.; Shi, P.-P. Two-Step Nonlinear Optical Switch in a Hydrogen-Bonded Perovskite-Type Crystal. *Chem. Commun.* **2022**, *58*, 1712−1715.
(18) Pan, C.-Y.; Yang, X.-R.; Xiong, L.; Lu, Z.-W.; Zhen, B.-Y.; Sui, X.; Deng, X.-B.; Chen, L.; Wu, L.-M. Solid-State Nonlinear Optical Switch with the Widest Switching Temperature Range Owing to Its Continuously Tunable T_c. *J. Am. Chem. Soc.* **2020**, *142*, 6423−6431.
(19) Botez, C. E.; Carbajal, D.; Adiraju, V. A. K.; Tackett, R. J.; Chianelli, R. R. Intermediate-Temperature Polymorphic Phase Transition in KH_2PO_4: A Synchrotron X-Ray Diffraction Study. *J. Phys. Chem. Solids* **2010**, *71*, 1576−1580.
(20) McMahon, M. I.; Nelmes, R. J.; Kuhs, W. F.; Dorwarth, R.; Piltz, R. O.; Tun, Z. Geometric Effects of Deuteration on Hydrogen-Ordering Phase Transitions. *Nature* **1990**, *348*, 317−319.
(21) Zachwieja, U.; Jacobs, H. Redetermination of the Crystal Structure of Diamine Silver(I)-Sulfate, $[Ag(NH_3)_2]_2SO_4$. *Z. Kristallogr.* **1992**, *201*, 207−212.
(22) Nose, S. A Unified Formulation of the Constant Temperature Molecular Dynamics Methods. *J. Chem. Phys.* **1984**, *81*, 511−519.
(23) Nose, S. Constant Temperature Molecular Dynamics Methods. *Prog. Theor. Exp. Phys.* **1991**, *103*, 1−46.
(24) Hoover, W. G. Canonical Dynamics: Equilibrium Phase-Space Distributions. *Phys. Rev. A* **1985**, *31*, 1695−1697.
(25) Kresse, G.; Furthmuller, J. Efficient Iterative Schemes for *ab initio* Total-energy Calculations Using a Plane-wave Basis Set. *Phys. Rev. B* **1996**, *54*, 11169−11186.
(26) Kohn, W. Nobel Lecture: Electronic Structure of Matter-Wave Functions and Density Functionals. *Rev. Mod. Phys.* **1999**, *71*, 1253−1266.
(27) Perdew, J. P.; Wang, Y. Accurate and Simple Analytic Representation of the Electron-Gas Correlation-Energy. *Phys. Rev. B* **1992**, *45*, 13244−13249.
(28) Kresse, G.; Joubert, D. From Ultrasoft Pseudopotentials to the Projector Augmented-Wave Method. *Phys. Rev. B* **1999**, *59*, 1758−1775.
(29) Laksari, S.; Chahed, A.; Abbouni, N.; Benhelal, O.; Abbar, B. First-Principles Calculations of the Structural, Electronic and Optical Properties of $CuGaS_2$ and $AgGaS_2$. *Comput. Mater. Sci.* **2006**, *38*, 223−230.
(30) Mo, S.-D.; Ching, W. Y. Electronic and Optical Properties of Three Phases of Titanium Dioxide: Rutile, Anatase, and Brookite. *Phys. Rev. B* **1995**, *51*, 13023−13032.
(31) Aversa, C.; Sipe, J. E. Nonlinear Optical Susceptibilities of Semiconductors: Results with a Length-Gauge Analysis. *Phys. Rev. B* **1995**, *52*, 14636−14645.
(32) Rashkeev, S. N.; Lambrecht, W. R. L.; Segall, B. Efficient *ab initio* Method for the Calculation of Frequency-Dependent Second-Order Optical Response in Semiconductors. *Phys. Rev. B* **1998**, *57*, 3905−3919.
(33) Fang, Z.; Lin, J.; Liu, R.; Liu, P.; Li, Y.; Huang, X.; Ding, K.; Ning, L.; Zhang, Y. Computational Design of Inorganic Nonlinear Optical Crystals Based on a Genetic Algorithm. *CrystEngComm* **2014**, *16*, 10569−10580.
(34) Shao, X.-D.; Zhang, X.; Shi, C.; Yao, Y.-F.; Zhang, W. Switching Dielectric Constant Near Room Temperature in a Molecular Crystal. *Adv. Sci.* **2015**, *2*, 1500029.
(35) Chen, T.; Sun, Z.; Zhao, S.; Ji, C.; Luo, J. An Organic-Inorganic Hybrid Co-Crystal Complex as a High-Performance Solid-State Nonlinear Optical Switch. *J. Mater. Chem. C* **2016**, *4*, 266−271.
(36) Sun, Z.; Chen, T.; Liu, X.; Hong, M.; Luo, J. Plastic Transition to Switch Nonlinear Optical Properties Showing the Record High Contrast in a Single-Component Molecular Crystal. *J. Am. Chem. Soc.* **2015**, *137*, 15660−15663.
(37) Katrusiak, A.; Szafranski, M. Ferroelectricity in NH···N Hydrogen Bonded Crystals. *Phys. Rev. Lett.* **1999**, *82*, 576−579.
(38) Wei, S.; Kong, X.; Wang, H.; Mao, Y.; Chao, M.; Guo, J.; Liang, E. Negative Thermal Expansion Property of $CuMoO_4$. *Optik* **2018**, *160*, 61−67.
(39) Liang, E.; Sun, Q.; Yuan, H.; Wang, J.; Zeng, G.; Gao, Q. Negative Thermal Expansion: Mechanisms and Materials. *Front Phys.* **2021**, *16*, 53302.
(40) Li, Q.; Lin, K.; Liu, Z.; Hu, L.; Cao, Y.; Chen, J.; Xing, X. Chemical Diversity for Tailoring Negative Thermal Expansion. *Chem. Rev.* **2022**, *122*, 8438−8486.
(41) Tan, G.; Zhao, L.-D.; Kanatzidis, M. G. Rationally Designing High-Performance Bulk Thermoelectric Materials. *Chem. Rev.* **2016**, *116*, 12123−12149.
(42) Qian, X.; Zhou, J.; Chen, G. Phonon-Engineered Extreme Thermal Conductivity Materials. *Nat. Mater.* **2021**, *20*, 1188−1202.
(43) Chen, H.; Yue, Z.; Ren, D.; Zeng, H.; Wei, T.; Zhao, K.; Yang, R.; Qiu, P.; Chen, L.; Shi, X. Thermal Conductivity during Phase Transitions. *Adv. Mater.* **2019**, *31*, 1806518.
(44) Liu, J.-Y.; Chen, L.; Wu, L.-M. Ag_9GaSe_6: High-Pressure-Induced Ag Migration Causes Thermoelectric Performance Irreproducibility and Elimination of such Instability. *Nat. Commun.* **2022**, *13*, 2966−2966.
(45) Li, L.; Liu, X.; Li, Y.; Xu, Z.; Wu, Z.; Han, S.; Tao, K.; Hong, M.; Luo, J.; Sun, Z. Two-Dimensional Hybrid Perovskite-Type Ferroelectric for Highly Polarization-Sensitive Shortwave Photodetection. *J. Am. Chem. Soc.* **2019**, *141*, 2623−2629.
(46) Xie, Y.; Zheng, J.; Zheng, K.; Liu, Q.; Duan, J.; Chen, W.; Shao, S.; Cai, H. High-Temperature Switchable Nonlinear Optical and Dielectric Material Revealed by Molecular Modification. *Chem. Mater.* **2021**, *33*, 3081−3086.
(47) Boixel, J.; Guerchais, V.; Le Bozec, H.; Jacquemin, D.; Amar, A.; Boucekkine, A.; Colombo, A.; Dragonetti, C.; Marinotto, D.; Roberto, D.; Righetto, S.; De Angelis, R. Second-Order NLO Switches from Molecules to Polymer Films based on Photochromic Cyclometalated Platinum(II) Complexes. *J. Am. Chem. Soc.* **2014**, *136*, 5367−5375.
(48) Loucif-Saibi, R.; Nakatani, K.; Delaire, J. A.; Dumont, M.; Sekkat, Z. Photoisomerization and Second Harmonic Generation in Disperse Red One-Doped and -Functionalized Poly(methyl methacrylate) Films. *Chem. Mater.* **1993**, *5*, 229−236.
(49) Boubekeur-Lecaque, L.; Coe, B. J.; Clays, K.; Foerier, S.; Verbiest, T.; Asselberghs, I. Redox-Switching of Nonlinear Optical Behavior in Langmuir-Blodgett Thin Films Containing a Ruthenium(II) Ammine Complex. *J. Am. Chem. Soc.* **2008**, *130*, 3286−3287.
(50) Shekaari, A.; Jafari, M. Finite Temperature Properties and Phase Transition Behavior of Quasi-Planar B_{36} Nanocluster from First Principles. *Mater. Res. Express* **2019**, *6*, 025014.

https://doi.org/10.1021/jacsau.2c00353
JACS Au 2022, 2, 2059−2067